MoS$_2$ Nanosheets−Cyanobacteria Interaction: Reprogrammed Carbon and Nitrogen Metabolism

Si Chen,[∇] Nibin Shi,[∇] Min Huang,[∇] Xianjun Tan, Xin Yan, Aodi Wang, Yuxiong Huang, Rong Ji, Dongmei Zhou, Yong-Guan Zhu, Arturo A. Keller, Jorge L. Gardea-Torresdey, Jason C. White, and Lijuan Zhao*

Read Online

ACCESS | Metrics & More | Article Recommendations | Supporting Information

ABSTRACT: Fully understanding the environmental implications of engineered nanomaterials is crucial for their safe and sustainable use. Cyanobacteria, as the pioneers of the planet earth, play important roles in global carbon and nitrogen cycling. Here, we evaluated the biological effects of molybdenum disulfide (MoS$_2$) nanosheets on a N$_2$-fixation cyanobacteria (*Nostoc sphaeroides*) by monitoring growth and metabolome changes. MoS$_2$ nanosheets did not exert overt toxicity to *Nostoc* at the tested doses (0.1 and 1 mg/L). On the contrary, the intrinsic enzyme-like activities and semiconducting properties of MoS$_2$ nanosheets promoted the metabolic processes of *Nostoc*, including enhancing CO$_2$-fixation-related Calvin cycle metabolic pathway. Meanwhile, MoS$_2$ boosted the production of a range of biochemicals, including sugars, fatty acids, amino acids, and other valuable end products. The altered carbon metabolism subsequently drove proportional changes in nitrogen metabolism in *Nostoc*. These intracellular metabolic changes could potentially alter global C and N cycles. The findings of this study shed light on the nature and underlying mechanisms of bio-nanoparticle interactions, and offer the prospect of utilization bio-nanomaterials for efficient CO$_2$ sequestration and sustainable biochemical production.

KEYWORDS: transition metal dichalcogenides, nanobio, cell factory, carbon sequestration, metabolic reprograming, carbon fixation
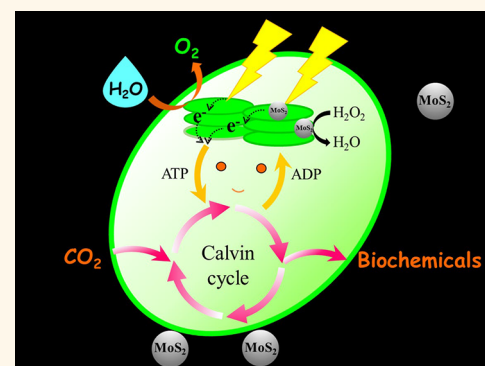
INTRODUCTION

Transition metal dichalcogenides (TMDs) are promising two-dimensional (2D) materials.[1] Molybdenum disulfide (MoS$_2$), as one of the most important TMDs, possesses excellent electrical, optical, electrochemical, and biological properties, which enable a wide variety of electronics, biomedicine, and energy applications.[2] In addition, the high density of active surface sites makes them ideal for biochemical sensing applications. MoS$_2$ can be used as biosensors for metabolites, nucleic acids, proteins, metal ions, and even a cell.[3] Recently, MoS$_2$ nanosheets have been used for environmental applications, including wastewater treatment, adsorption, photocatalysis, membrane-based separation, and disinfection.[4] The increasing use of MoS$_2$ nanomaterials, especially in the environmental field, will likely lead to the significant release of MoS$_2$ nanosheets into the environment.[5] Thus, understanding the environmental behavior and biological effects of this material is critically important for its safe and sustainable use.

Cyanobacteria were the first organisms that performed oxygenic photosynthesis on earth and are commonly assumed to be a critical node in the evolution of life.[6] In addition to their roles in evolution, cyanobacteria are major drivers of the biogeochemical cycling of carbon (C) and nitrogen (N).[7] It is estimated that 20−30% organic carbon on the earth is derived from photosynthetic carbon fixation by cyanobacteria.[8] In addition, cyanobacteria are the primary N$_2$-fixing microorganisms in marine environments.[9] Cyanobacteria inhabit diverse aquatic and terrestrial environments,[10] ensuring significant coexisting and interaction with natural or engineered nanomaterials. Given the important ecological
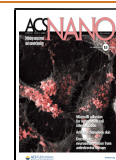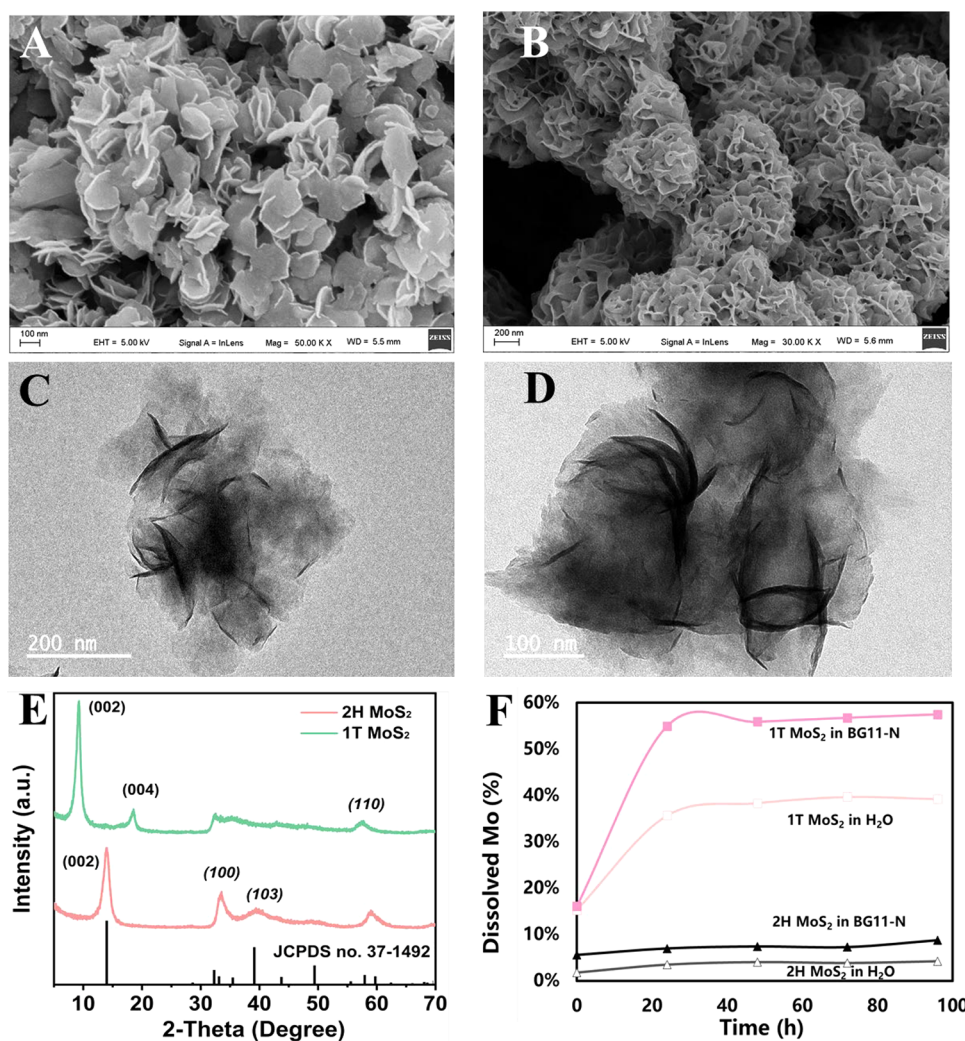
Figure 1. Characterization of 1T and 2H MoS$_2$ nanosheets. (A and B) SEM images of 1T and 2H MoS$_2$ nanosheets, displaying a typical flower-like morphology of both phases of MoS$_2$. (C and D) TEM images of 1T and 2H MoS$_2$. (E) XRD pattern of 1T and 2H MoS$_2$ nanosheets. (F) Dissolution rate of 1T and 2H MoS$_2$ nanosheets in water and BG11-N growth media over 96 h.

function of cyanobacteria, investigating the environmental implication of nanomaterials such as MoS$_2$ nanosheets on cyanobacteria is of great importance.

In terms of cellular interactions, nanoscale particles are known to penetrate lipid bilayers of cell membrane.[11] As such, MoS$_2$ nanosheets may penetrate cyanobacterial cells, and the diverse surface chemistry of this material makes interaction with biological molecules highly likely. Cao *et al.*[12] have shown that MoS$_2$@HSA can rapidly interact with blood proteins and immune cells. In addition, MoS$_2$ nanosheets have semiconducting properties, and in nature, semiconducting nanomaterials are similar to chlorophyll molecules in that both materials can be excited by photons, generating photoexcited electrons. The relatively small band gap (1.3 eV) of MoS$_2$ allows most of the solar spectrum to be harvested. As such, MoS$_2$ nanosheets located in thylakoid membrane have the potential to help cyanobacteria harvest greater energy per photon. Recent studies have revealed that semiconductors can transfer photogenerated electrons to non-photosynthetic bacteria, promoting their growth and cellular metabolism.[13−16] Whether additional solar energy from semiconducting nanomaterials can be harvested and be used to stimulate the metabolism of cyanobacteria accordingly remains largely

unknown. In addition, MoS$_2$ nanosheets can be oxidized by O$_2$ environmentally, subsequently releasing Mo ions,[17] and given that Mo is a required nutrient, these released ions may induce certain biological processes.[18,19] The changes of metabolism induced by either nanoparticulate or ionic Mo will be reflected by the metabolite profile of the cell. Metabolites are the end products of cellular metabolic reactions, and changes in the metabolite profile can represent a complex network of biological events that reflect the physiologic state of the organism.[20] Therefore, metabolomics, studying the complete set of metabolites, offers a snapshot of cellular physiology in response to MoS$_2$ nanosheet exposure.

In the present study, we investigated the biological effects of two phases of MoS$_2$ nanosheets (1T and 2H) on a N$_2$-fixing cyanobacteria (*Nostoc sphaeroides* (*N. sphaeroides*)). *Nostoc* were exposed to different concentrations (0, 0.1, and 1 mg/L) of 1T or 2H MoS$_2$ for 96 h. The impacts of MoS$_2$ on the growth of *Nostoc* was evaluated by determining the optical density at 680 nm (OD 680), chlorophyll content, and dry weight. Meanwhile, gas chromatography−mass spectrometry (GC-MS) based metabolomics was used to evaluate changes in the metabolome, and the mechanistic significance of these changes as a function of MoS$_2$ exposure was evaluated. This
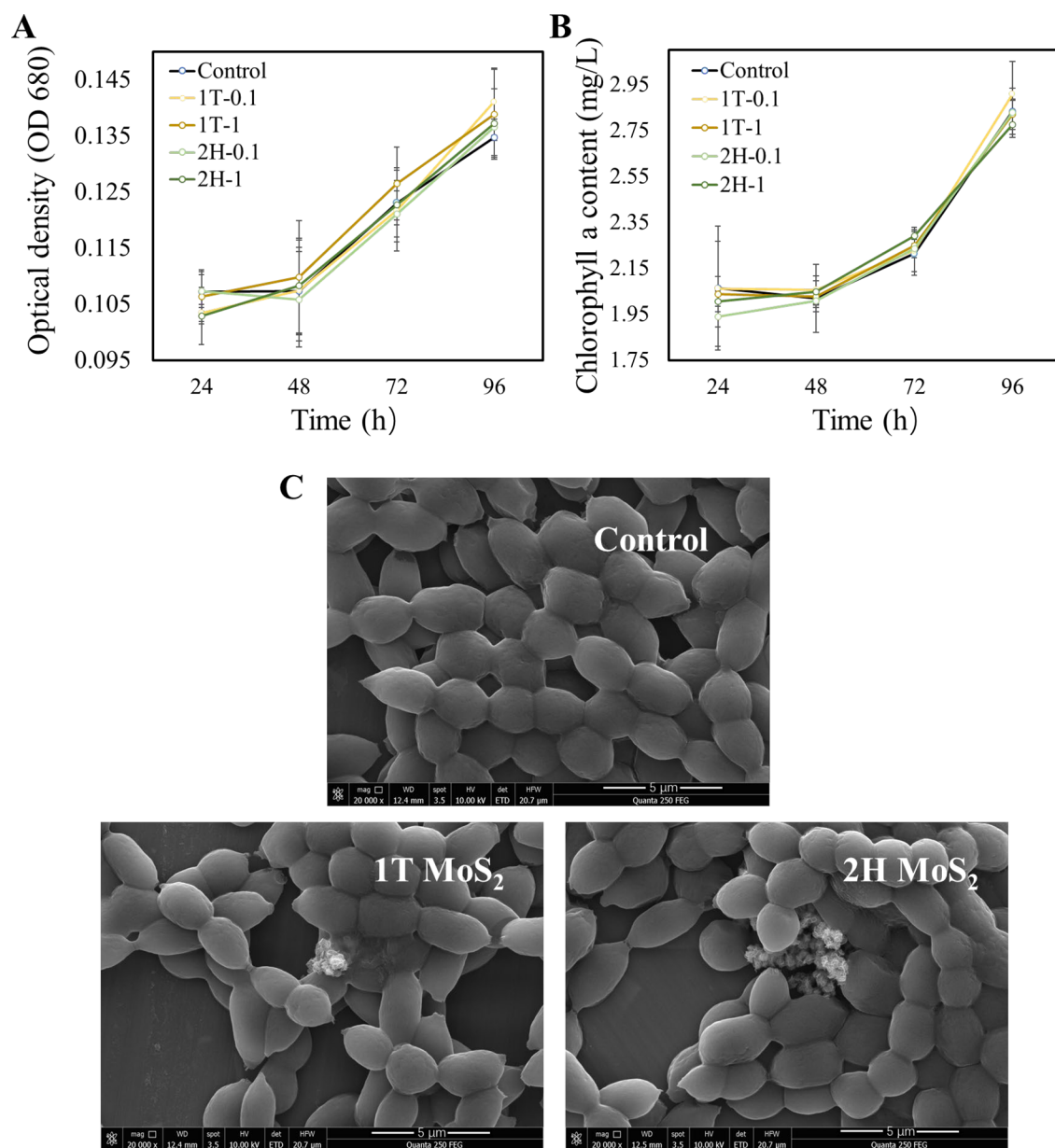
Figure 2. Effect of MoS$_2$ nanosheets on the growth of cyanobacteria (*Nostoc sphaeroides*). (A) Biomass (reflected by OD 680) and (B) chlorophyll *a* content of cyanobacteria exposed to different concentrations of 1T or 2H MoS$_2$ at two concentrations (0.1 and 1 mg/L) for 96 h. Data are average of three replicates. (C) SEM images of control cyanobacteria and MoS$_2$−cyanobacteria.

study provides valuable information on the environmental risk of MoS$_2$ nanosheets.

RESULTS AND DISCUSSION

Characteristics of MoS$_2$ Nanosheets. The scanning electron microscopy (SEM) images show that both 1T and 2H MoS$_2$ nanosheets possessed a flake-like morphology (Figure 1A,B). The transmission electron microscopy (TEM) images further confirmed the ultrathin nanosheet structures of 1T and 2H MoS$_2$ (Figure 1C,D). TEM images also reveal that the mean sizes for 1T and 2H MoS$_2$ nanosheets are 150 ± 20 and 350 ± 50 nm, which suggest that the 2H phase MoS$_2$ nanosheets have a larger size compared to 1T MoS$_2$. The crystal phases of 2H and 1T MoS$_2$ nanosheets were characterized by X-ray diffraction. The characteristic peaks for 2H MoS$_2$ are evident by the XRD patterns (Figure 1E), while the (002) peak of 1T MoS$_2$ shifts to a lower degree of

9.3°, accompanying the formation of a second-order peak at 18.6°. This phenomenon was associated with newly formed lamellar structure with enlarged interlayer spacing by NH$_4^+$, which was consistent with previous reports.[21] The diffraction pattern of trigonal prismatic (2H) and octahedral (1T) MoS$_2$ nanosheets was consistent with the diffraction pattern originally presented by Zhu *et al.*[22] Dynamic light scattering (DLS) analysis revealed hydrodynamic diameters of 1T and 2H MoS$_2$ in nanopore water of 312 ± 38 and 947 ± 6 nm, respectively, with ζ potential values of 5.6 ± 0.46 and 6.0 ± 3.9 mV, respectively. These indicate the significant difference in size but not charge between two phases of MoS$_2$ nanosheets.

Dissolution of MoS$_2$ Nanosheets. The degradation and dissolution behavior of nanomaterials in the environment is of critical importance for assessing the environmental fate and biological effects.[23] Thus, the dissolution of MoS$_2$ nanosheets in both water and cultivation medium (BG11-N) was

monitored over 96 h. As shown in Figure 1F, metallic 1T MoS₂ nanosheets have a much greater dissolution rate than that of 2H MoS₂ in both water and BG11-N media. At 96 h, the dissolution rate of 1T MoS₂ reached 23.5 and 34.6% in water and BG11-N, respectively. This indicates that 1T MoS₂ is relatively unstable in the environment, producing a pool of soluble Mo ions that will coexist with particulate MoS₂ in environmental media. Therefore, 1T MoS₂ nanosheets will pose both a "nanospecific" risk and Mo ions risk to receptors. In contrast, 2H MoS₂ nanosheets are more stable, with dissolution rates of 2.4 and 4.8% in water and BG11-N, respectively. Thus, material-specific or nanospecific effects will be dominant for 2H MoS₂ nanosheets when released into the environment. The dissolution is mediated through oxidation of the MoS₂ nanosheets, and the released soluble species is molybdate ion (MoO_4^{2-}).[24]

Influence of MoS₂ Nanosheets on *Nostoc* Growth. The growth rate of *Nostoc* was monitored *via* measuring OD 680 at 24 h intervals over 96 h. The results show that OD 680 were unchanged upon exposure to either MoS₂ nanosheet (1T and 2H) at either dose (Figure 2A). Chlorophyll *a* levels are another standard method for determining growth rates of photosynthetic organisms.[25] The chlorophyll *a* growth curve shows that exposure to MoS₂ nanosheets did not impact pigment content (Figure 2B). Malondialdehyde (MDA) is the product of lipid peroxidation of the cell membrane, and its content reflects the degree of oxidative damage. Supporting Information Figure S1 shows that MDA content was unchanged upon exposure to MoS₂ nanosheets, indicating no oxidative stress was induced. SEM micrographs show that *Nostoc* cells cultivated with 1T or 2H MoS₂ appeared intact, indicating no damage to the cell membrane (Figure 2C). Together, these findings suggest that both phases of MoS₂ nanosheets exerted minimal negative impacts on *Nostoc* growth.

GC-MS-Based Metabolomics. Although MoS₂ nanosheets did not exert overt toxicity to *Nostoc*, the materials' complex surface chemistry enables interaction with intracellular biomolecules, potentially affecting the metabolism of *Nostoc*. In order to evaluate the potentially altered biochemical pathways, GC-MS-based metabolomics was performed.[26] By using GC-MS, 294 metabolites were identified and semi-quantified in *Nostoc* cells. In order to assess the variation of the measured metabolome between groups, multivariate sparse partial least-squares-discriminant analysis (sPLS-DA) was performed. The score plot indicates good separation of the four MoS₂ groups (*Nostoc* in the presence of MoS₂) from the control group (*Nostoc* in the absence of MoS₂; Figure 3A). These data indicate that both phases of MoS₂ nanosheets altered the metabolite profile of *Nostoc*, and the alteration occurred in a somewhat dose-dependent manner. Generally, 2H MoS₂ nanosheets induced more pronounced metabolic changes than did 1T MoS₂ at the same dose. To focus on the most important features that contributed to the separation between MoS₂ groups and the control group, metabolites with a sPLS-DA VIP score > 0.1 were selected for the final discriminant feature list (Figure 3B). A total of 43 metabolic features significantly distinguished the MoS₂ and control groups. Interestingly, all of these metabolites were up-regulated upon MoS₂ exposure. The relative abundance of these metabolites followed a uniform pattern: 2H MoS₂ at 1 mg/L > 2H MoS₂ at 0.1 mg/L > 1T MoS₂ at 1 mg/L > 1T MoS₂ at 0.1 mg/L > Control. This systematic positive modulation of
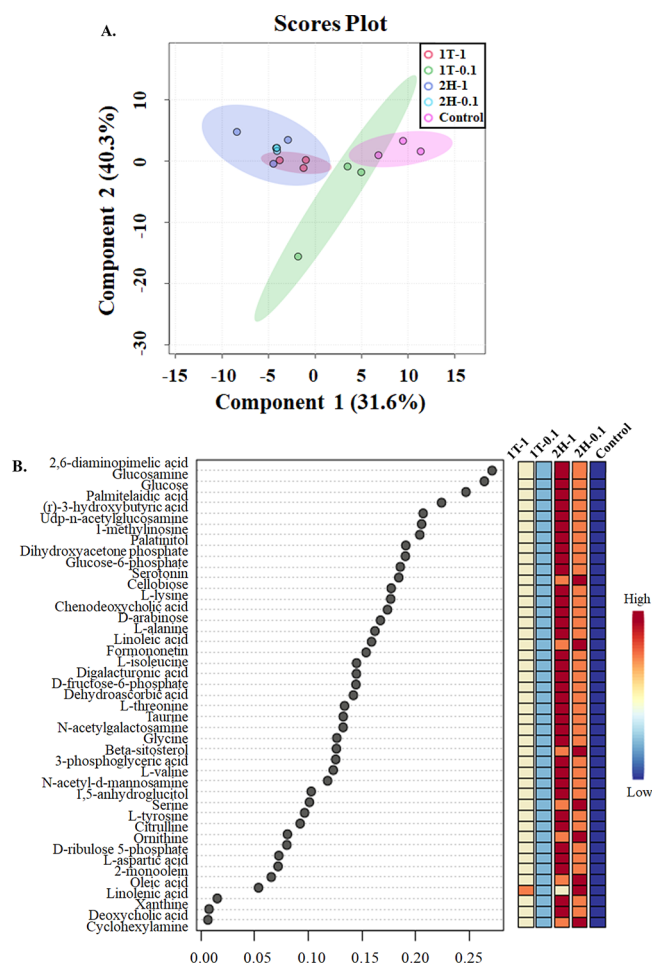

Figure 3. Multivariate analysis of metabolomics data obtained by GC-MS. (A) Sparse partial least-squares discriminate analysis (sPLS-DA) score plots of metabolic profiles in cyanobacteria treated without and with different concentrations of 1T or 2H MoS₂ at 0.1 and 1 mg/L. (B) VIP score plot showing the metabolome pattern in five groups (control, 1T MoS₂ at 0.1 mg/L, 1T MoS₂ at 1 mg/L, 2H MoS₂ at 0.1 mg/L, and 2H MoS₂ at 1 mg/L). Cyanobacteria (*Nostoc sphaeroides*) were cultivated in BG11-N growth media for 96 h.

metabolic processes in *Nostoc* driven by MoS₂ is both interesting and promising. This suggests that MoS₂ at both doses are generally beneficial for *Nostoc* metabolism. In addition, our previous study found that antioxidant related metabolites, such as phenolic acids and polyphenols, are very sensitive to environmental stressors. For example, Ag NPs at 0.1 mg/L resulted in a considerable decrease of antioxidant compounds.[27] In contrast, all of the detected antioxidants in *Nostoc*, including catechin, 4-hydroxycinnamic acid, resveratrol, 1,2,4-benzenetriol, epicatechin, pelargonic acid, 3,4-dihydroxycinnamic acid, chlorogenic acid, and α-tocopherol, were unaffected upon MoS₂ exposure (data not shown). This indicates that MoS₂ had limited impacts on oxidative stress in *Nostoc*, which is consistent with the above-mentioned data on MDA and the growth rate.

Carbon Metabolism. It is noteworthy that several key intermediates in the Calvin cycle were significantly increased upon MoS₂ exposure, including D-glyceraldehyde-3-phosphate (G3P, 2−7-fold), dihydroxyacetone phosphate (DHAP, 2−10-fold), 3-phosphoglyceric acid (3-PGA, 1−6-fold), D-ribulose-5-
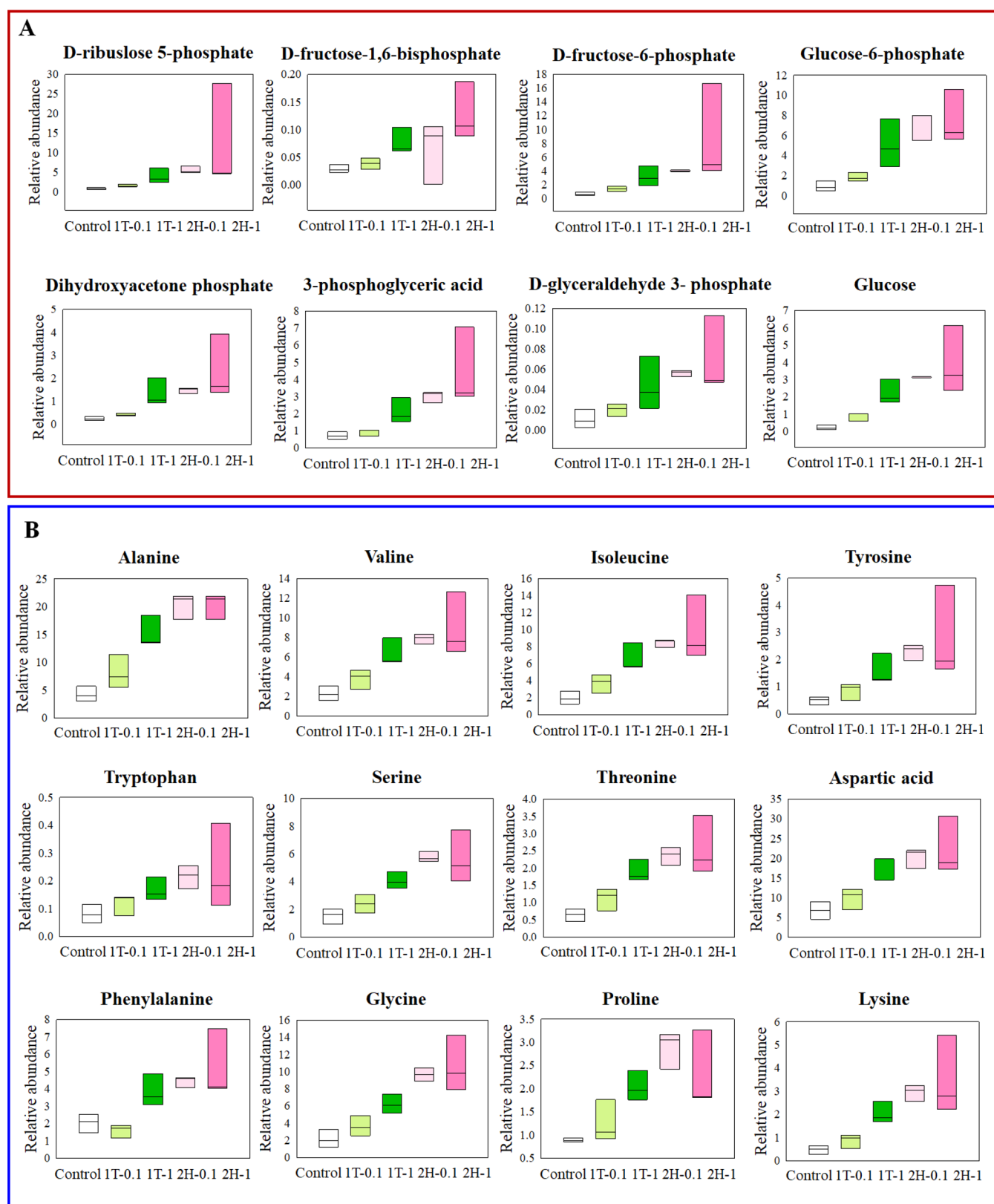
Figure 4. Significantly changed carbon and nitrogen related metabolites in *Nostoc*. Box plot showing the relative abundance of Calvin cycle associated metabolites (A) and amino acids (B). *Nostoc* were cultivated in BG11-N growth media with different concentrations of 1T or 2H MoS$_2$ for 96 h.

phosphate (Ru-5-P, 2−13-fold), D-fructose-1,6-bisphosphate (FBP, 1−4-fold), D-fructose-6-phosphate (F-6-P, 2−12-fold), and glucose-6-phosphate (G-6-P, 2−8-fold) (see box plot in

Figure 4A). In addition, the final product of the Calvin cycle, glucose, was significantly increased by 3−16-fold upon exposure to two phases of MoS$_2$ nanosheets at both
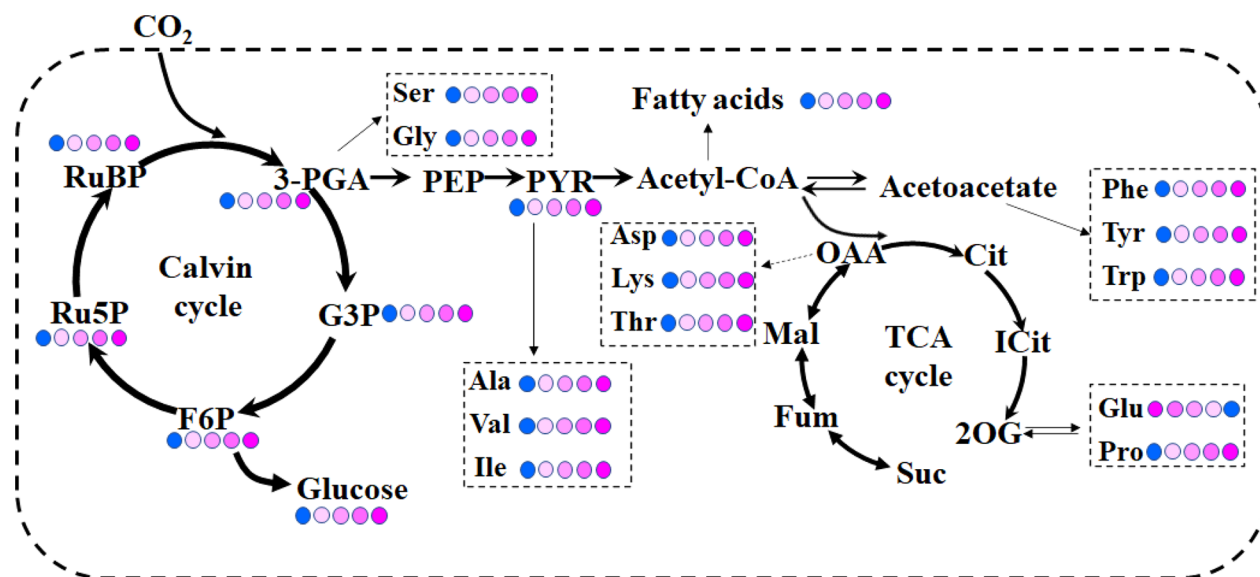
Figure 5. Metabolic pathways involved in carbon and nitrogen metabolism in cyanobacteria (*Nostoc sphaeroides*). Pathways were generated by mapping labeled metabolites onto known metabolic pathways. Each arrow shows the direction of the reaction. RuBP, ribulose 1,5-bisphosphate; Ru5P, D-ribulose-5-phosphate; F6P, D-fructose-6-phosphate; G3P, glyceraldehyde-3-phosphate; 3-PGA, 3-phosphoglyceric acid; PEP, phosphoenolpyruvate; Pyr, pyruvate; Cit, citrate; ICit, isocitrate; 2-OG, 2-oxoglutarate; SSA, succinic semialdehyde; Suc, succinate; Fum, fumarate; Mal, malate; Arg, arginine; His, histidine; Pro, proline; Glu, glutamic acid; Gln, glutamine; Ile, isoleucine; Met, methionine; Val, valine; Phe, phenylalanine; Tyr, tyrosine.

concentrations (Figure 4A). For photosynthetic microorganisms, the Calvin cycle is the sole CO_2-fixation pathway, in which CO_2 is reduced into carbohydrate metabolites.[28] The up-regulation of Calvin cycle intermediates may suggest that both semiconducting 2H MoS_2 and metallic 1T MoS_2 nanosheets can augment CO_2-fixation pathways in *Nostoc*, although the mechanisms by which MoS_2 exposure could enhance the CO_2 fixtion of *Nostoc* are unknown. In marine, freshwater, and terrestrial environments, *Nostoc*, being an important N_2-fixing cyanobacteria, could have close contact with natural or engineered MoS_2 nanosheets; and this environmental interaction could significantly alter carbon metabolism of the *Nostoc*. In a non-photosynthetic bacteria (*Moorella thermoacetica*), the carbon-fixation-related Wood–Ljungdahl metabolic pathway has been found to be activated by CdS nanoparticles.[13] Importantly, this augmented carbon fixation was attributed to semiconducting properties of CdS. Under light illumination, photoelectrons excited from semiconducting CdS provided additional reducing power for the bacteria. In the current study, the underlying mechanism for the MoS_2-enabled reprogramming of the carbon metabolism is unknown but could be related to a similar boosting of intracellular reducing power.

Biochemicals Production. Bacteria invest fixed carbon into growth, survival, and the generation of new biomass.[29] Given that *Nostoc* species are filamentous, the OD value cannot accurately reflect the actual biomass. Thus, dry weight was determined by a microbalance (Mettle Toledo XP56) in order to know whether MoS_2 exposure increased the biomass of *Nostoc*. Results show that the biomass did not differ between groups, although 2H MoS_2 at 0.1 mg/L did increase biomass, albeit it in a statistically insignificant fashion (Figure S2). This suggests that *Nostoc* did not use the fixed carbon for biomass accumulation but, instead, maintained the population and directed excess carbon into alternative metabolic pathways, potentially enhancing the production of various biochemicals.

For instance, several important carbohydrates such as maltotriose, cellobiose, arabinose, and palatinitol were increased 1.5–5.6-fold upon MoS_2 exposure (Figure S3). Moreover, a number of unsaturated fatty acids and their precursors, including myristic acid (17–32%), palmitic acid (30–83%), palmitelaidic acid (2–10-fold), oleic acid (3–12-fold), linoleic acid (4–13-fold), linolenic acid (5–9-fold), behenic acid (31–57%), lignoceric acid (15–50%), and 2-monoolein (1.6–3.7-fold) were significantly increased upon exposure to MoS_2 nanosheets (Figure S4). This indicates that MoS_2 exposure boosted fatty acid biosynthesis in *Nostoc*. Fatty acids are valuable biofuels, and genetically modified cyanobacteria have been used to increase the fatty acid production for this purpose.[30]

In addition to fatty acids, we found that exposure to both 1T and 2H MoS_2 significantly increased the synthesis of a variety of valuable biochemicals. For example, (*r*)-3- hydroxybutyric acid (3HB), a precursor to synthesize biodegradable plastics poly(hydroxyalkanoates) (PHAs) and many related chemicals,[31] was increased 2.5–6.9-fold upon exposure to MoS_2 nanosheets. Myo-inositol is a precursor for many valuable chemicals used in the functional food and pharmaceutical industry;[32] the abundance of myo-inositol increased 20–38-fold upon exposure to MoS_2 nanosheets. In addition, D-myo-inositol-4-phosphate, the downstream product of myo-inositol, increased 603–1620-fold compared to unamended controls. Additionally, high-value metabolites such as glucosamine (5–18-fold), dehydroascorbic acid (DHA, 7.5–36 fold), cheno-deoxycholic acid (CDCA, 1.8–5.9-fold), β-sitosterol (6–21-fold), and formononetin (FMT, 1.5–6.7-fold) were all significantly increased upon exposure to MoS_2 (Figure S5); these high-value-added compounds are widely used in the cosmetics, pharmaceutical, and food industries.[33] Taken together, these findings demonstrate that MoS_2 nanosheets exhibit great potential to augment photosynthetic CO_2 fixation and biochemicals production; this systemic MoS_2-driven
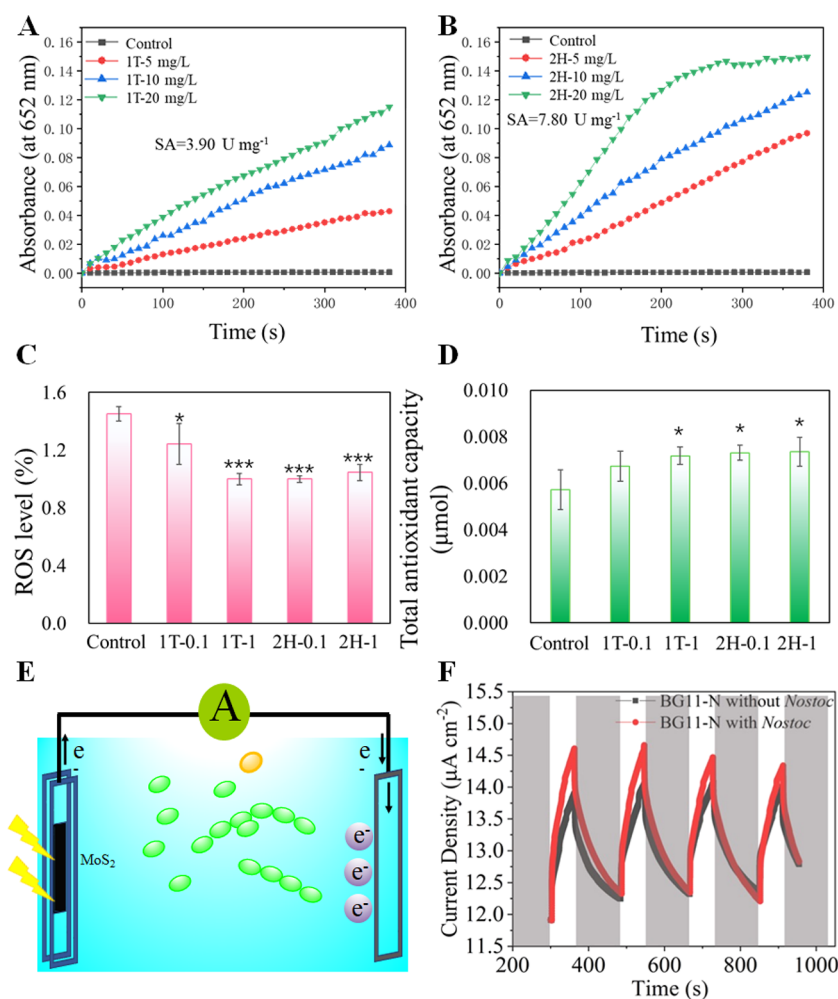
Figure 6. Antioxidant enzyme-mimicking properties and semiconducting activities of MoS_2 nanosheets. (A and B) POD-like activities of 1T and 2H MoS_2. (C and D) Levels of ROS and total antioxidant capacities in cyanobacteria (*Nostoc sphaeroides*) exposed to different concentrations (0.1 and 1 mg/L) of 1T or 2H MoS_2 nanosheets for 96 h. (E) Schematic diagram of the electron transferring process between 2H MoS_2 nanosheet and cyanobacteria under visible light irradiation. (F) Transition photocurrent of MoS_2 and MoS_2−cyanobacteria system under light on/off cycles.

increase in cyanobacterial metabolic output has far reaching implications.

Cyanobacteria are usually regarded as promising cell factories;[34] they can fix atmospheric CO_2 and simultaneously produce hydrogen[35,36] and other valuable chemicals and biofuels through endogenous metabolic pathways.[37] However, low solar to energy conversion efficiencies and limited light harvesting capacity remain as critical bottlenecks for the commercial application of cyanobacteria-based cellular factories.[38] To date, metabolic engineering and synthetic biology are strategies commonly used to accelerate metabolism and improve the efficiency of cellular factories.[39,40] Compared to genetic engineering to alter specific metabolic pathways, exogenous nanomaterial stimulation to modulate bacterial metabolism is a more straightforward and potentially more robust platform for efficient and sustainable CO_2 capture and large-scale biochemicals production.

Nitrogen Metabolism. Certain cyanobacteria can perform oxygenic photosynthesis and nitrogen fixation simultaneously,[41,42] including the selected *Nostoc* in this study. Importantly, a number of amino acids and their derivatives were significantly increased in *Nostoc* in the presence of 1T or 2H MoS_2 nanosheets (Figure 4B, box plot). Serine and glycine,

both of which are related to photosynthetic respiration, were significantly increased by 1.6−3.7-fold and 1.7−4.9-fold, respectively, upon exposure to MoS_2 nanosheets. In addition, amino acids derived from pyruvate, including alanine (1.9−5.4-fold), valine (0.68−2.9-fold), and isoleucine (0.88−3.9-fold), were all significantly elevated by MoS_2. Amino acids derived from oxaloacetate (OAA), such as aspartic acid (0.46−2.3-fold), lysine (0.83−6.3-fold), and threonine (0.74−3.0-fold), were also elevated upon exposure to MoS_2. Proline, derived from 2-oxoglutarate (2OG), was significantly increased 1.4−2.6-fold compared to control. Phenylalanine, tyrosine, and tryptophan serve as precursors for important secondary metabolites related antioxidant activity[43] and were all also significantly increased. The relative abundance of these significantly changed amino acids followed the same pattern: 2H MoS_2 at 1 mg/L > 2H MoS_2 at 0.1 mg/L > 1T MoS_2 at 1 mg/L > 1T MoS_2 at 0.1 mg/L > Control (Figure 4B), which is very similar to that of the carbon-related metabolites.

The increases in amino acids levels suggest that MoS_2 nanosheets could have increased N_2 fixation. As such, we determined the total nitrogen content in *Nostoc* in the absence and in the presence of MoS_2 nanosheets. Surprisingly, the total N level remained unchanged regardless of nanosheet type or

dose (Figure S6). Thus, an alternative mechanism for the increased amino acid production must be at play. Nitrogen metabolism is closely linked with carbon metabolism through the tricarboxylic acid (TCA) cycle (Figure 5). Since MoS_2 nanosheets enhanced carbon-fixation-related metabolic pathways, *Nostoc* likely enhanced nitrogen (amino acid) assimilation to keep pace with increased CO_2 fixation, because the metabolism needs to balance the C/N ratio.[44,45] In summary, MoS_2 exposure enhanced carbon fixation and subsequently altered nitrogen metabolism. Given the important ecological function of cyanobacteria, these cellular changes in C and N metabolism are notable and, at a large scale, could potentially influence global biogeochemical cycling of C and N.[46]

Mechanism for MoS_2 Induced Metabolic Reprogramming in *Nostoc*. The above results indicate that both 1T and 2 H MoS_2 nanosheets at relatively low dose (0.1 mg/L) profoundly reprogrammed the central carbon metabolism in *Nostoc*. We are curious about the underlying mechanism for this significant and potentially important metabolome shift. Both the nanomaterial itself and Mo ions released from the nanosheets may contribute to the observed biological response of the *Nostoc*. Given the fact that 1T phase MoS_2 with higher dissolution rate (supplying more Mo ions) induced much less pronounced metabolic changes compared to 2H phase MoS_2, we consider the mechanism by which MoS_2 nanosheets reprogram *Nostoc* metabolism to be more strongly linked to the nanoscale material, instead of Mo ions. To verify this hypothesis, additional experiments were conducted to test whether Mo ions can induce similar metabolic reprogramming. *Nostoc* were then cultivated in BG11-N growth media amended with different concentrations (0, 4.5, and 9 μg/L) of Mo ions ($Na_2MoO_4 \cdot 2H_2O$) for 96 h, and the collected *Nostoc* cells were subjected to the metabolomics analysis as described above. Importantly, neither the unsupervised PCA nor the supervised PLS-DA model detected any significant separation between the Mo ion groups and control group (Figure S7), indicating that Mo ions did not shift the *Nostoc* metabolome. All metabolites (Calvin cycle related metabolites, fatty acids, and amino acids) that were found to be significantly increased upon exposure to MoS_2 nanosheets remained unaffected by MoO_4^{2-} treatment. These results clearly indicate that the significant metabolic reprogramming of *Nostoc* driven by MoS_2 nanosheets is not due to the released Mo ions but is a function of the nanoscale properties of this important material, although Mo is an essential element and participates in a wide range of metabolic processes.

Thus, it is likely that small-sized MoS_2 nanostructures gain the entry into the cells, and once there, certain intrinsic biological and optical−electrical properties of MoS_2 nanostructures directly drive the metabolic changes. Chen *et al.*[47] showed that MoS_2 nanosheets possess intrinsic multienzyme-mimicking activities, including superoxide dismutase (SODs), catalases (CATs), and peroxidases (PODs), under physiological conditions (pH 7.4, 25 °C). Thus, MoS_2 nanosheets possess ROS (reactive oxygen species) scavenging activities. For oxygenic photosynthetic organisms, ROS are inevitably generated by photosynthetic electron transport.[48] When the excitation of photosynthetic pigments exceeds metabolic demand, subsequent electron transfer reactions can lead to ROS generation.[49] Light-driven electron transport transfers electrons from the acceptor site of photosystem I (PSI) to various acceptors in the membrane, including oxygen. For example, there is direct electron transfer from reduced

ferredoxin to O_2, generating superoxide radicals (O_2^-).[50] The generated ROS may induce oxidative damage, diminishing photosynthetic efficiencies. As such, if MoS_2 nanosheets with antioxidant capacities reach the thylakoid membrane, it may improve the redox status of PSII and PSI embedded in the membrane by scavenging ROS and subsequently increase photosynthetic efficiency. To verify these hypotheses, we first determined the POD-. CAT-, and SOD-like activities of both phases of MoS_2 nanosheets. Results showed that 1T and 2H MoS_2 nanosheets exert weak CAT- (Figure S8) and no SOD-mimicking activity (data not shown). However, both 1T and 2H MoS_2 nanosheets exhibit excellent POD enzyme-mimicking activities (Figure 6A,B), which can catalyze detoxification of H_2O_2 to H_2O. It is noteworthy that 2H MoS_2 possessed greater POD-mimicking activities and also resulted in more pronounced metabolic reprogramming as compared to 1T MoS_2. This may indicate that the enhancement of CO_2 fixation is tightly linked to the intrinsic catalytic activities of MoS_2. The underlying mechanism for MoS_2 nanosheets has POD-mimicking activities is attributed to the electron transferring capacities of the nanomaterial.[47] Both Mo^{4+} and Mo^{6+} exist on the surface of the MoS_2 nanosheets, and the nanomaterial can act as an electron shuttle between the two valences. We further determined ROS levels in *Nostoc* exposed to different concentrations of 1T or 2H MoS_2 nanosheets. Interestingly, exposure to both phases of MoS_2 nanosheets significantly decreased intracellular ROS levels ($p < 0.05$, t test) as shown by the conversion of the dye 2′-7′dichlorofluorescin diacetate (DCFH-DA) to its fluorescent form 2′-7′dichlorofluorescein (DCF) (Figure 6C). This indicates that MoS_2 nanosheets can lower ROS levels in *Nostoc* cells. Total antioxidant capacity (TAC) is an important parameter for assessing antioxidant potential.[51] In the presence of MoS_2 nanosheets, the TAC was significantly ($p < 0.05$, t test) increased by 25.7 to 28.7% (Figure 6D). On the basis of these results, we speculate that MoS_2 nanosheets may enhance the efficiency of the light reactions by catalyzing the conversion of H_2O_2 to H_2O in light reaction center. The light reaction supplies the energy and reducing power (ATP and NADPH) for the subsequent carbon-fixation stage of photosynthesis, boosting the Calvin cycle.

In addition to enzyme-mimicking activities, 2H MoS_2 also possess excellent optical and electronic properties. The small band gap (1.3 eV) makes MoS_2 capable of harvesting much of the solar spectrum.[4] Under illumination, the intracellular semiconducting MoS_2 nanosheets can absorb light and generate photoexcited electrons that may be transferred to the electron transport chain of photosynthetic machinery and supply reducing powder for *Nostoc*. In Giraldo *et al.*,[11] semiconducting single-walled carbon nanotubes (SWNTs) were shown to promote the photosynthetic activity of chloroplasts. The explanation for the photosynthetic enhancement by SWNTs was attributed to electron transfer between SWNTs and the chloroplast. On the other hand, extracellular large-sized MoS_2 nanosheets may also have the possibility to transfer the photoelectrons to *Nostoc*, providing the reducing power for *Nostoc* metabolism. To verify this hypothesis, a light−MoS_2−*Nostoc* reaction system was established in a single chamber to enable measurement of key photoelectrochemical parameters (Figure 6E). Under light illumination, the MoS_2−*Nostoc* hybrid exhibited greater photocurrent density (6.12%; Figure 6F), suggesting that a photoenhanced
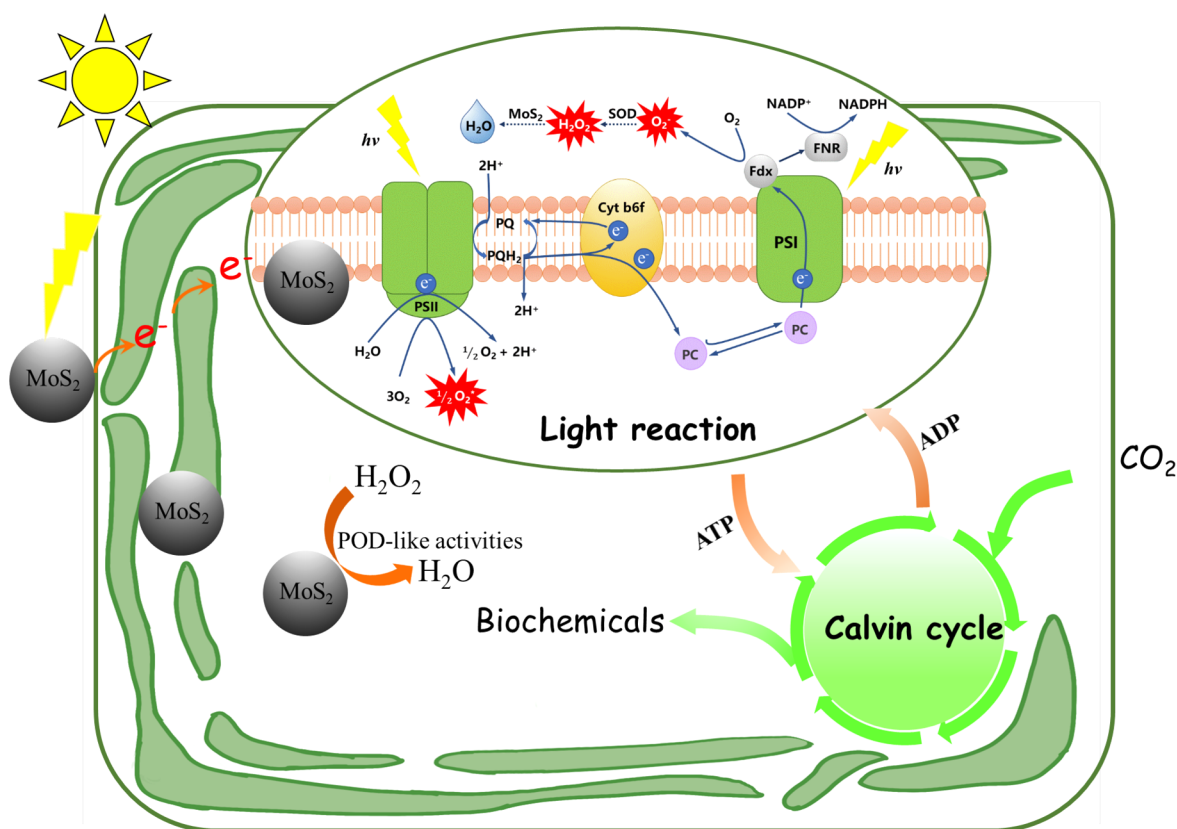
Figure 7. Schematic illustration of the mechanisms for MoS_2 nanosheets enhancing CO_2 fixation in cyanobacteria (*Nostoc sphaeroides*). MoS_2 nanosheets effectively catalyze the degradation of H_2O_2 into H_2O and O_2. The POD-mimicking activities enable MoS_2 nanosheets to augment the efficiency of the light reaction, which subsequently enhances carbon fixation. Another pathway by which 2H MoS_2 enhances carbon fixation is through the nanomaterials semiconducting properties, which deliver photoelectrons to the cyanobacteria cells, supplying the reducing power for general metabolic processes.

extracellular electron transfer process was occurring from the semiconducting nanomaterial to the *Nostoc* cells.

In summary, the enhanced CO_2 fixation and biochemical production upon exposure to MoS_2 is likely the result of the intrinsic catalytic and optical−electrical activities of MoS_2 nanosheets, instead of the released Mo ions. Figure 7 summarized the proposed pathways for MoS_2 nanosheets altering metabolic processes in *Nostoc*.

CONCLUSIONS

The findings of this study have important implications for understanding the interaction between nanomaterials and photosynthetic microorganisms. First, we found that MoS_2 exposure at low dose (0.1 mg/L) can dramatically reprogram carbon and nitrogen metabolism of *Nostoc*, an important N_2-fixation cyanobacteria. In modern oceans, the release of anthropogenic nanomaterials is increasing due to the wide application of nanotechnology across an array of sectors. Cyanobacteria occupy a broad range of habitats across fresh water, marine, and terrestrial environments. This enables significantly cyanobacterial interaction with the discharged nanomaterials. Thus, nanomaterials with exceptional physicochemical properties may alter the elemental biogeochemical cycles *via* reprogramming intracellular metabolism. Second, we found that MoS_2 nanosheets exposure can boost the CO_2-fixation-related Calvin cycle and can subsequently enhance the production of valuable biochemicals. Thus, the MoS_2−*Nostoc* system might be an alternative approach for atmospheric CO_2

capture and simultaneous efficient microbial cell factory functions, providing a sustainable strategy to alleviate critical environmental and energy problems. Third, using the catalytic active sites of nanomaterials to accelerate metabolism of bacteria might be a straightforward approach to promote the efficiency of cyanobacteria-based cell factory beyond metabolic engineering and synthetic biology. Mechanistic investigations related to CO_2 fixation and the potential to exploit these critical metabolic outputs are currently underway, especially to use ^{13}C-labeled metabolic flux analysis to accurately evaluate the carbon fixation and metabolism process.

METHODS

Preparation and Characterization of MoS_2 Nanosheets. MoS_2 nanosheets with hexagonal (2H phase) or octahedral (1T phase) crystal structures were prepared according to Liu *et al.*[52] 2H MoS_2 nanosheets were prepared by a facile hydrothermal method. Initially, 0.5 mmol of $(NH_4)_6Mo_7O_{24} \cdot 4H_2O$ and 0.85 mmol of thiourea were dissolved in 35 mL of H_2O. After stirring for 30 min, the solution was transferred into a 50 mL Teflon-lined stainless-steel autoclave and kept at 220 °C for 24 h. After the autoclave was cooled to room temperature, the products were collected by centrifugation (13000 rpm, 20 min), washed with distilled water and ethanol for several times, and dried at 60 °C under vacuum. 1T MoS_2 nanosheets were prepared by a similar procedure except 1 mmol of $(NH_4)_6Mo_7O_{24} \cdot 4H_2O$ and 30 mmol of thiourea were used.

Field emission scanning electron microscopy (FE-SEM) images were obtained on a Hitachi SU8010 microscope (Japan). High-resolution transmission electron microscopy (HRTEM) was also conducted (FEI Tecnai G2F30 Netherland). X-ray diffraction (XRD)

was conducted on using a Bruker D8 diffractometer with Cu Kα X-rays. Raman spectra were from a Horiba Jobin spectrometer. The hydrodynamic diameter and ζ potential of the MoS$_2$ nanosheets in ultrapure water was measured *via* dynamic light scattering (DLS; Zetasizer Nano ZS, Malvern). A MoS$_2$ stock suspension of 0.1 mg/L for DLS analysis was sonicated (KH-100DB, Hechuang Utrasonic, Jiangsu, China) at 45 kHz for 30 min to obtain a well dispersed suspension.

MoS$_2$ Nanosheet Dissolution Experiment. The dissolution of Mo ions from 1T and 2H MoS$_2$ nanosheets was done in deionized water and in the cultivation solution (BG11-N). Specifically, 1 mg of the 1T or 2H phase of MoS$_2$ was added to 100 mL of deionized water or BG11-N solution, followed by incubation for 96 h. Samples were collected at 20 min and 24, 48, 72, and 96 h. At each sampling time, 10 mL of suspension was transferred into a centrifugal ultrafilter (MAP003C38, 3 kDa, Pall, USA), followed by centrifugation at 8000g for 20 min to isolate released Mo ions. Four replicates were used in each treatment at each time point. The collected supernatant was acidified by concentrated HNO$_3$ prior to quantification of Mo by inductively coupled plasma−optical emission spectroscopy (ICP-OES; PQ 9000, Analytik Jena).

***Nostoc* Culture and Growth Conditions.** *Nostoc sphaeroides* cyanobacteria were obtained from the Institute of Wuhan Hydrobiology, Chinese Academy of Sciences. The initial density was 1 × 10^6 *Nostoc* cells mL^{-1}. BG11-N (composition in Table S1) was used as growth medium for *Nostoc*'s routine culture. Notably, given that one of the purposes of the study was to determine the impact of MoS$_2$ on N$_2$ fixation, the growth medium of BG11-N is deficient in nitrogen. If a N source (NO$_3^-$ or NH$_4^+$) is abundant in the growth medium, nitrogenase will remain inactive, and the N$_2$ fixation is likely to be inhibited to a certain degree. The cyanobacteria were cultured at 25 ± 1 °C using a 12 h/12 h light/dark cycle under continuous cool light fluorescent lights with a total light intensity of 36 μM photons·m^{-2}·s^{-1}.

Growth Rate and MDA Content of *Nostoc*. The *Nostoc* cell optical densities (biomass) were determined at 680 nm (OD 680) using a microplate spectrophotometer (Varioskan LUX, Thermo Scientific, America) according to the manufacturer's instructions. Chlorophyll content was determined according to Sigalat *et al.*[53] The thiobarbituric acid-reactive substances (TBARS) assay was used to determine MDA content as a measure of lipid peroxidation in cyanobacteria.[54] Briefly, 1 mL of cyanobacterial cells was mixed with 2 mL of 10% trichloroacetic acid, and then centrifuged at 10000g for 15 min. A 1 mL supernatant was added to 3 mL of 0.67% thiobarbituric acid; the mixture was heated in a water bath at 95 °C for 30 min. After cooling, the absorbance at 450, 532, and 600 nm was measured with a microplate reader (Synergy H4 Hybrid Reader, BioTek, America).

SEM Observation of MoS$_2$−Cyanobacteria. The morphology of cyanobacteria cells and the distribution of MoS$_2$ on the cell surface were observed using SEM (FEI Quanta 250 FEG) equipped with an energy dispersive X-ray spectroscopy (EDS; Oxford Aztec X-ManN80). Briefly, the samples were fixed in 2.5% glutaraldehyde, dehydrated in gradient concentrations of ethanol, and coated with a layer of gold, and then the images were observed and analyzed for MoS$_2$ distribution using SEM and EDS.

Quantification of Metabolites in Nostoc Using GC-MS. MoS$_2$ nanosheets (2H phase) at 0.1 mg/L were added to the cyanobacteria growth media (BG11-N, Table S1), followed by cultivation for 96 h. The extraction of metabolites from cyanobacteria cells and subsequent GC-MS quantification were conducted according to the protocol reported previously. Briefly, the cells (15 mL) were collected by centrifugation (3000 rpm, 20 min) for metabolome analysis. The cell pellets were then washed 3 times with PBS buffer. Subsequently, the washed cell pellets were immediately frozen in liquid nitrogen for 20s for complete metabolic inactivation.[55] The frozen samples were stored at −80 °C. The metabolites were extracted from deep-frozen cells using 1 mL of 80% methanol containing a defined amount of the internal standard 2-chloro-L-phenylalanine (0.3 mg·mL^{-1}) and 200 μL of chloroform to extract lipophilic metabolites. The mixtures were sonicated for 30 min followed by centrifugation. The collected

supernatant was vacuum freeze-dried. The extracted compounds were derivatized using methoxylamine hydrochloride and *N*,*O*-bis-(trimethylsilyl) trifluoroacetamide (BSTFA). An Agilent 7890B gas chromatograph coupled to an Agilent 5977A mass selective detector (Santa Clara, CA, USA), with a DB-5MS fused-silica capillary column (30 m × 0.25 mm internal diameter with 0.25 μm film; Agilent J & W Scientific, Folsom, CA, USA), was used to analyze the samples. Quantification was reported as peak height using the unique ion as default. Metabolites were unambiguously assigned by the BinBase identifier numbers using retention index and mass spectrum as the two most important identification criteria. More details regarding sample derivatization and GC-MS analysis are referenced in a previous study.[56]

Metabolomics Data Analysis. For GC-MS data, a supervised sparse partial least-squares discriminant analysis (sPLS-DA) clustering method was run *via* online resources (http://www.metaboanalyst.ca/).[57] Before sPLS-DA, data normalization (normalization by sum) was performed for general-purpose adjustment on the basis of the differences among samples, and data transformation (log transformation) was conducted to make individual features more comparable. The variable importance in projection (VIP) is the weighted sum of the squares of the sPLS-DA analysis, which indicates the importance of a variable to the entire model.[58] A variable with a VIP greater than 0.1 is regarded as responsible for separation and is defined as a discriminating metabolite in this study.[59] Biological pathway analysis was performed on the basis of the GC-MS data using MetaboAnalyst 2.0.[60] The library used in pathway analysis is the *Chlorella variabilis* (green alga) KEGG pathway. The impact value threshold calculated for pathway identification was set at 0.1.[59]

Total Nitrogen Determination. The total nitrogen in the cyanobacteria was determined *via* persulfate oxidation.[61] A 5 mL aliquot of cyanobacteria was placed in a colorimetric tube and diluted to 10 mL, followed by the addition of 5 mL of alkaline potassium persulfate (40 g of K$_2$S$_2$O$_8$ and 15 g of NaOH in 1 L of H$_2$O). The plug was tightened, and the sample was heated in a sterilizing pan (120−124 °C, 30 min). Samples were then cooled to room temperature, followed by the addition of 1 mL of HCl (37% HCl:H$_2$O = 1:9) and dilution to 25 mL. The absorbance was measured at 220 and 275 nm using a UV spectrophotometer (UV2310II, Techcomp, China), with the calculation formula being $A = A_{220} − 2A_{275}$. A set of known concentrations of potassium nitrate (KNO$_3$) (0, 1, 2, 4, 6, 10, 14, and 16 mg/L) were used to prepare a standard curve.

Antioxidant Enzymes-Mimicking Activities of MoS$_2$ Nanosheets. The CAT-like catalytic performance of MoS$_2$ nanosheets was evaluated according to Liu *et al.*[62] The superoxide dismutase (SOD)-mimicking activities of MoS$_2$ nanosheets were measured using SOD colorimetric activity kit (Nanjing Jiancheng Bioengineering Institute, Nanjing, China). The peroxidase-like (POD-like) catalytic activity of MoS$_2$ nanosheets was determined using a nanozyme-catalyzed colorimetric reaction according to Jiang *et al.*[63] More details of these protocols are provided in the Supporting Information.

ROS and Total Antioxidant Capacities in *Nostoc*. The level of ROS in cyanobacterial cells was determined suing 2′,7′-dichlorodihydrofluorescein diacetate (H$_2$DCFDA) as a fluorescence probe.[64] Cyanobacteria (2 mL) were centrifuged at 4 °C for 900g for 30 min, the supernatant was removed, 1 mL of Tris-HCl (10 mM) was added, and the sample was centrifuged again. Then 100 μL of supernatant was added to 800 μL of Tris-HCl (10 mM) and 100 μL of H$_2$DCFDA (100 μm) and incubated at 37 °C for 30 min. The fluorescence signal was monitored with a microplate reader (Synergy H4 Hybrid Reader, BioTek, America) using an excitation wavelength of 488 nm and an emission wavelength of 525 nm.

The antioxidant capacity of *Nostoc* was assessed by ferric-reducing antioxidant power (FRAP) assay.[65] First, the FRAP reagent was prepared freshly by mixing 300 mM acetate buffer (pH 3.6) with 10 mM tripyridyl-*s*-triazine (TPTZ) solution in 40 mM HCl and 20 mM FeCl$_3$·6H$_2$O in 10:1:1 ratio and kept at 37 °C. Then 10 mL of cyanobacterial cells were centrifuged at 900g for 30 min, the supernatant was removed, 1.5 mL of extracting agent (80% acetone

and ethanol; 1:1) was added to the precipitate, and the sample was extracted at 4 °C for 12 h in dark. The sample was then centrifuged at 1000g for 15 min, and to 50 μL of sample extract was added 1.5 mL of FRAP reagent. The samples were mixed and store in the dark at 37 °C for 4−5 h prior to measuring the absorbance of the mixture at 593 nm. A set of known concentrations of ferrous sulfate ($FeSO_4$) (0, 0.125, 0.25, 0.5, 1, and 2 mM) were prepared for a standard curve. The values obtained were expressed as mM of ferrous ($Fe(II)$) equivalent.

Statistical Analysis. For all data except GG-MS-based metabolomics data, a student's t test was performed to evaluate the significance in the difference between the MoS_2 group and Control.

ASSOCIATED CONTENT

Ⓢ Supporting Information

The Supporting Information is available free of charge at https://pubs.acs.org/doi/10.1021/acsnano.1c05656.

Assay for determination of enzyme activities; (Table S1) BG11-N growth medium composition; (Figure S1) MDA content of *Nostoc*; (Figure S2) MoS_2 nanosheet exposure effects; (Figures S3−S5) relative abundance amounts; (Figure S6) total nitrogen content; (Figure S7) PCA and PLS-DA score plot; (Figure S8) activities of MoS_2 nanosheets (PDF)

AUTHOR INFORMATION

Corresponding Author

Lijuan Zhao − *State Key Laboratory of Pollution Control and Resource Reuse, School of the Environment, Nanjing University, Nanjing 210023, China;* ◉ orcid.org/0000-0002-8481-0435; Email: ljzhao@nju.edu.cn

Authors

Si Chen − *State Key Laboratory of Pollution Control and Resource Reuse, School of the Environment, Nanjing University, Nanjing 210023, China*

Nibin Shi − *State Key Laboratory of Pollution Control and Resource Reuse, School of the Environment, Nanjing University, Nanjing 210023, China*

Min Huang − *State Key Laboratory of Pollution Control and Resource Reuse, School of the Environment, Nanjing University, Nanjing 210023, China*

Xianjun Tan − *Shenzhen Environmental Science and New Energy Technology Engineering Laboratory, Tsinghua-Berkeley Shenzhen Institute (TBSI), Tsinghua Shenzhen International Graduate School, Tsinghua University, Shenzhen 518055, China*

Xin Yan − *State Key Laboratory of Pollution Control and Resource Reuse, School of the Environment, Nanjing University, Nanjing 210023, China*

Aodi Wang − *State Key Laboratory of Pollution Control and Resource Reuse, School of the Environment, Nanjing University, Nanjing 210023, China*

Yuxiong Huang − *Shenzhen Environmental Science and New Energy Technology Engineering Laboratory, Tsinghua-Berkeley Shenzhen Institute (TBSI), Tsinghua Shenzhen International Graduate School, Tsinghua University, Shenzhen 518055, China;* ◉ orcid.org/0000-0001-8124-643X

Rong Ji − *State Key Laboratory of Pollution Control and Resource Reuse, School of the Environment, Nanjing University, Nanjing 210023, China;* ◉ orcid.org/0000-0002-1724-5253

Dongmei Zhou − *State Key Laboratory of Pollution Control and Resource Reuse, School of the Environment, Nanjing University, Nanjing 210023, China;* ◉ orcid.org/0000-0002-7917-7954

Yong-Guan Zhu − *Key Laboratory of Urban Environment and Health, Institute of Urban Environment, Chinese Academy of Sciences, Xiamen 361021, China*

Arturo A. Keller − *Chemistry and Biochemistry Department, The University of Texas at El Paso, El Paso, Texas 79968, United States;* ◉ orcid.org/0000-0002-7638-662X

Jorge L. Gardea-Torresdey − *Bren School of Environmental Science & Management and Center for Environmental Implications of Nanotechnology, University of California, Santa Barbara, California 93106, United States;* ◉ orcid.org/0000-0002-9467-0536

Jason C. White − *The Connecticut Agricultural Experiment Station (CAES), New Haven, Connecticut 06504, United States;* ◉ orcid.org/0000-0001-5001-8143

Complete contact information is available at:
https://pubs.acs.org/10.1021/acsnano.1c05656

Author Contributions

▽S.C., N.S., and M.H. contributed equally to this work.

Notes

The authors declare no competing financial interest.

REFERENCES

(1) Li, Y.; Dietrich, S.; Forsythe, C.; Taniguchi, T.; Watanabe, K.; Moon, P.; Dean, C. R. Anisotropic Band Flattening in Graphene with One-Dimensional Superlattices. *Nat. Nanotechnol.* **2021**, *16* (5), 525−530.

(2) Manzeli, S.; Ovchinnikov, D.; Pasquier, D.; Yazyev, O. V.; Kis, A. 2D Transition Metal Dichalcogenides. *Nat. Rev. Mater.* **2017**, *2* (8), 17033.

(3) Bolotsky, A.; Butler, D.; Dong, C.; Gerace, K.; Glavin, N. R.; Muratore, C.; Robinson, J. A.; Ebrahimi, A. Two-Dimensional Materials in Biosensing and Healthcare: From *in Vitro* Diagnostics to Optogenetics and Beyond. *ACS Nano* **2019**, *13* (9), 9781−9810.

(4) Wang, Z.; Mi, B. Environmental Applications of 2D Molybdenum Disulfide (MoS_2) Nanosheets. *Environ. Sci. Technol.* **2017**, *51* (15), 8229−8244.

(5) Nowack, B.; Bucheli, T. D. Occurrence, Behavior and Effects of Nanoparticles in the Environment. *Environ. Pollut.* **2007**, *150* (1), 5−22.

(6) Lyons, T. W.; Reinhard, C. T.; Planavsky, N. J. The Rise of Oxygen in Earth's Early Ocean and Atmosphere. *Nature* **2014**, *506* (7488), 307−315.

(7) Sigman, D. M.; Boyle, E. A. Glacial/Interglacial Variations in Atmospheric Carbon Dioxide. *Nature* **2000**, *407* (6806), 859−869.

(8) Waterbury, J. B.; Watson, S. W.; Guillard, R. R. L.; Brand, L. E. Widespread Occurrence of a Unicellular, Marine, Planktonic, Cyanobacterium. *Nature* **1979**, *277* (5694), 293−294.

(9) Zehr, J. P. Nitrogen Fixation by Marine Cyanobacteria. *Trends Microbiol.* **2011**, *19* (4), 162−173.

(10) Chen, M.-Y.; Teng, W.-K.; Zhao, L.; Hu, C.-X.; Zhou, Y.-K.; Han, B.-P.; Song, L.-R.; Shu, W.-S. Comparative Genomics Reveals Insights into Cyanobacterial Evolution and Habitat Adaptation. *ISME J.* **2021**, *15* (1), 211−227.

(11) Giraldo, J. P.; Landry, M. P.; Faltermeier, S. M.; McNicholas, T. P.; Iverson, N. M.; Boghossian, A. A.; Reuel, N. F.; Hilmer, A. J.; Sen, F.; Brew, J. A.; Strano, M. S. Plant Nanobionics Approach to Augment Photosynthesis and Biochemical Sensing. *Nat. Mater.* **2014**, *13* (4), 400−408.

(12) Cao, M.; Cai, R.; Zhao, L.; Guo, M.; Wang, L.; Wang, Y.; Zhang, L.; Wang, X.; Yao, H.; Xie, C.; Cong, Y.; Guan, Y.; Tao, X.; Wang, Y.; Xu, S.; Liu, Y.; Zhao, Y.; Chen, C. Molybdenum Derived from Nanomaterials Incorporates into Molybdenum Enzymes and Affects Their Activities *in Vivo*. *Nat. Nanotechnol.* **2021**, *16* (6), 708−716.

(13) Sakimoto, K. K.; Wong, A. B.; Yang, P. Self-Photosensitization of Nonphotosynthetic Bacteria for Solar-to-Chemical Production. *Science* **2016**, *351* (6268), 74−77.

(14) Guo, J.; Suástegui, M.; Sakimoto, K. K.; Moody, V. M.; Xiao, G.; Nocera, D. G.; Joshi, N. S. Light-Driven Fine Chemical Production in Yeast Biohybrids. *Science (Washington, DC, U. S.)* **2018**, *362* (6416), 813−816.

(15) Zhang, H.; Liu, H.; Tian, Z.; Lu, D.; Yu, Y.; Cestellos-Blanco, S.; Sakimoto, K. K.; Yang, P. Bacteria Photosensitized by Intracellular Gold Nanoclusters for Solar Fuel Production. *Nat. Nanotechnol.* **2018**, *13* (10), 900−905.

(16) Lu, A.; Li, Y.; Jin, S.; Wang, X.; Wu, X.-L.; Zeng, C.; Li, Y.; Ding, H.; Hao, R.; Lv, M.; Wang, C.; Tang, Y.; Dong, H. Growth of Non-phototrophic Microorganisms Using Solar Energy through Mineral Photocatalysis. *Nat. Commun.* **2012**, *3*, 768.

(17) Lee, T.-W.; Chen, C.-C.; Chen, C. Chemical Stability and Transformation of Molybdenum Disulfide Nanosheets in Environmental Media. *Environ. Sci. Technol.* **2019**, *53* (11), 6282−6291.

(18) Schwarz, G.; Mendel, R. R.; Ribbe, M. W. Molybdenum Cofactors, Enzymes and Pathways. *Nature* **2009**, *460* (7257), 839−847.

(19) Cao, M.; Cai, R.; Zhao, L.; Guo, M.; Wang, L.; Wang, Y.; Zhang, L.; Wang, X.; Yao, H.; Xie, C.; Cong, Y.; Guan, Y.; Tao, X.; Wang, Y.; Xu, S.; Liu, Y.; Zhao, Y.; Chen, C. Molybdenum Derived from Nanomaterials Incorporates into Molybdenum Enzymes and Affects Their Activities *in Vivo*. *Nat. Nanotechnol.* **2021**, *16* (6), 708−716.

(20) Annibal, A.; Tharyan, R. G.; Schonewolff, M. F.; Tam, H.; Latza, C.; Auler, M. M. K.; Gronke, S.; Partridge, L.; Antebi, A. Regulation of the One Carbon Folate Cycle as a Shared Metabolic Signature of Longevity. *Nat. Commun.* **2021**, *12* (1), 3486.

(21) Liu, Q.; Li, X.; He, Q.; Khalil, A.; Liu, D.; Xiang, T.; Wu, X.; Song, L. Gram-Scale Aqueous Synthesis of Stable Few-Layered 1T-MoS$_2$: Applications for Visible-Light-Driven Photocatalytic Hydrogen Evolution. *Small* **2015**, *11* (41), 5556−5564.

(22) Zhu, W.; Zhang, L.; Zhang, W.; Zhang, F.; Li, Z.; Zhu, Q.; Qi, S. Facile Synthesis of GNPs@NixSy@MoS$_2$ Composites with Hierarchical Structures for Microwave Absorption. *Nanomaterials* **2019**, *9* (10), 1403.

(23) Chen, X.; Shinde, S. M.; Dhakal, K. P.; Lee, S. W.; Kim, H.; Lee, Z.; Ahn, J.-H. Degradation Behaviors and Mechanisms of MoS$_2$ Crystals Relevant to Bioabsorbable Electronics. *NPG Asia Mater.* **2018**, *10* (8), 810−820.

(24) Wang, Z.; Von dem Bussche, A.; Qiu, Y.; Valentin, T. M.; Gion, K.; Kane, A. B.; Hurt, R. H. Chemical Dissolution Pathways of MoS$_2$ Nanosheets in Biological and Environmental Media. *Environ. Sci. Technol.* **2016**, *50* (13), 7208−7217.

(25) Herrmann, A. J.; Sorwat, J.; Byrne, J. M.; Frankenberg-Dinkel, N.; Gehringer, M. M. Diurnal Fe(II)/Fe(III) Cycling and Enhanced O$_2$ Production in a Simulated Archean Marine Oxygen Oasis. *Nat. Commun.* **2021**, *12* (1), 2069.

(26) Sperber, H.; Mathieu, J.; Wang, Y.; Ferreccio, A.; Hesson, J.; Xu, Z.; Fischer, K. A.; Devi, A.; Detraux, D.; Gu, H.; Battle, S. L.; Showalter, M.; Valensisi, C.; Bielas, J. H.; Ericson, N. G.; Margaretha, L.; Robitaille, A. M.; Margineantu, D.; Fiehn, O.; Hockenbery, D.; et al. The Metabolome Regulates the Epigenetic Landscape During Naive-to-Primed Human Embryonic Stem Cell Transition. *Nat. Cell Biol.* **2015**, *17* (12), 1523−1535.

(27) Huang, M.; Keller, A. A.; Wang, X.; Tian, L.; Wu, B.; Ji, R.; Zhao, L. Low Concentrations of Silver Nanoparticles and Silver Ions Perturb the Antioxidant Defense System and Nitrogen Metabolism in N$_2$-Fixing Cyanobacteria. *Environ. Sci. Technol.* **2020**, *54* (24), 15996−16005.

(28) Tamoi, M.; Miyazaki, T.; Fukamizo, T.; Shigeoka, S. The Calvin Cycle in Cyanobacteria Is Regulated by CP12 *via* the NAD(H)/NADP(H) Ratio under Light/Dark Conditions. *Plant J.* **2005**, *42* (4), 504−513.

(29) Angermayr, S. A.; Gorchs Rovira, A.; Hellingwerf, K. J. Metabolic Engineering of Cyanobacteria for the Synthesis of Commodity Products. *Trends Biotechnol.* **2015**, *33* (6), 352−361.

(30) Liu, X.; Sheng, J.; Curtiss, R., III Fatty Acid Production in Genetically Modified Cyanobacteria. *Proc. Natl. Acad. Sci. U. S. A.* **2011**, *108* (17), 6899−6904.

(31) Wang, B.; Pugh, S.; Nielsen, D. R.; Zhang, W.; Meldrum, D. R. Engineering Cyanobacteria for Photosynthetic Production of 3-Hydroxybutyrate Directly from CO$_2$. *Metab. Eng.* **2013**, *16*, 68−77.

(32) Wang, X.; Chen, L.; Liu, J.; Sun, T.; Zhang, W. Light-Driven Biosynthesis of *myo*-Inositol Directly From CO$_2$ in *Synechocystis* sp. PCC 6803. *Front. Microbiol.* **2020**, *11* (2435), 566117.

(33) Lu, Y.; Wang, L.; Teng, F.; Zhang, J.; Hu, M.; Tao, Y. Production of Myo-Inositol from Glucose by a Novel Trienzymatic Cascade of Polyphosphate Glucokinase, Inositol 1-Phosphate Synthase and Inositol Monophosphatase. *Enzyme Microb. Technol.* **2018**, *112*, 1−5.

(34) Kanno, M.; Carroll, A. L.; Atsumi, S. Global Metabolic Rewiring for Improved CO$_2$ Fixation and Chemical Production in Cyanobacteria. *Nat. Commun.* **2017**, *8* (1), 14724.

(35) Appel, J.; Hueren, V.; Boehm, M.; Gutekunst, K. Cyanobacterial *in Vivo* Solar Hydrogen Production Using a Photosystem I-Hydrogenase (PsaD-HoxYH) Fusion Complex. *Nat. Energy* **2020**, *5* (6), 458−467.

(36) Benemann, J. R.; Weare, N. M. Hydrogen Evolution by Nitrogen-Fixing *Anabaena cylindrica* Cultures. *Science* **1974**, *184* (4133), 174−175.

(37) Zhang, A.; Carroll, A. L.; Atsumi, S. Carbon Recycling by Cyanobacteria: Improving CO$_2$ Fixation through Chemical Production. *FEMS Microbiol. Lett.* **2017**, *364* (16), fnx165.

(38) Zhou, Y. J.; Kerkhoven, E. J.; Nielsen, J. Barriers and Opportunities in Bio-Based Production of Hydrocarbons. *Nat. Energy* **2018**, *3* (11), 925−935.

(39) Claassens, N. J.; Sousa, D. Z.; Dos Santos, V. A.; De Vos, W. M.; Van Der Oost, J. Harnessing the Power of Microbial Autotrophy. *Nat. Rev. Microbiol.* **2016**, *14* (11), 692−706.

(40) Rasala, B. A.; Mayfield, S. P. Photosynthetic Biomanufacturing in Green Algae; Production of Recombinant Proteins for Industrial, Nutritional, and Medical Uses. *Photosynth. Res.* **2015**, *123* (3), 227−239.

(41) Singh, J. S.; Kumar, A.; Rai, A. N.; Singh, D. P. Cyanobacteria: A Precious Bio-resource in Agriculture, Ecosystem, and Environmental Sustainability. *Front. Microbiol.* **2016**, *7*, 529.

(42) Rai, A. N.; Singh, A. K.; Syiem, M. B. Plant Growth-Promoting Abilities in Cyanobacteria. *Cyanobacteria: From Basic Science to Applications*, 1st ed.; Academic Press: Cambridge, MA, USA, 2019; Chapter 23, 459−476. DOI: 10.1016/B978-0-12-814667-5.00023-4G.

(43) Maeda, H.; Dudareva, N. The Shikimate Pathway and Aromatic Amino Acid Biosynthesis in Plants. *Annu. Rev. Plant Biol.* **2012**, *63*, 73−105.

(44) Herrero, A.; Muro-Pastor, A. M.; Flores, E. Nitrogen Control in Cyanobacteria. *J. Bacteriol.* **2001**, *183* (2), 411−425.

(45) Forchhammer, K.; Selim, K. A. Carbon/Nitrogen Homeostasis Control in Cyanobacteria. *FEMS Microbiol. Rev.* **2020**, *44* (1), 33−53.

(46) Elbert, W.; Weber, B.; Burrows, S.; Steinkamp, J.; Büdel, B.; Andreae, M. O.; Pöschl, U. Contribution of Cryptogamic Covers to the Global Cycles of Carbon and Nitrogen. *Nat. Geosci.* **2012**, *5* (7), 459−462.

(47) Chen, T.; Zou, H.; Wu, X.; Liu, C.; Situ, B.; Zheng, L.; Yang, G. Nanozymatic Antioxidant System Based on MoS_2 Nanosheets. *ACS Appl. Mater. Interfaces* **2018**, *10* (15), 12453−12462.

(48) Latifi, A.; Ruiz, M.; Zhang, C.-C. Oxidative Stress in Cyanobacteria. *FEMS Microbiol. Rev.* **2009**, *33* (2), 258−278.

(49) Roach, T.; Krieger-Liszkay, A. Photosynthetic Regulatory Mechanisms for Efficiency and Prevention of Photo-Oxidative Stress. *Annu. Plant Rev. Online* **2019**, *2* (1), 273−306.

(50) Baier, M.; Dietz, K.-J. Chloroplasts as Source and Target of Cellular Redox Regulation: A Discussion on Chloroplast Redox Signals in the Context of Plant Physiology. *J. Exp. Bot.* **2005**, *56* (416), 1449−1462.

(51) Feng, W.; Han, X.; Hu, H.; Chang, M.; Ding, L.; Xiang, H.; Chen, Y.; Li, Y. 2D Vanadium Carbide MXenzyme to Alleviate ROS-Mediated Inflammatory and Neurodegenerative Diseases. *Nat. Commun.* **2021**, *12* (1), 2203.

(52) Liu, Q.; Li, X.; He, Q.; Khalil, A.; Liu, D.; Xiang, T.; Wu, X.; Song, L. Gram-Scale Aqueous Synthesis of Stable Few-Layered 1T-MoS_2: Applications for Visible-Light-Driven Photocatalytic Hydrogen Evolution. *Small* **2015**, *11* (41), 5556−5564.

(53) Huang, M.; Keller, A. A.; Wang, X.; Tian, L.; Wu, B.; Ji, R.; Zhao, L. Low Concentrations of Silver Nanoparticles and Silver Ions Perturb the Antioxidant Defense System and Nitrogen Metabolism in N_2-Fixing Cyanobacteria. *Environ. Sci. Technol.* **2020**, *54* (24), 15996−16005.

(54) Jambunathan, N.Determination and Detection of Reactive Oxygen Species (ROS), Lipid Peroxidation, and Electrolyte Leakage in Plants. *Plant Stress Tolerance*; Methods in Molecular Biology (Methods and Protocols); Humana Press, 2010; Vol. *639*, pp 292−298. DOI: 10.1007/978-1-60761-702-0_18.

(55) Schwarz, D.; Nodop, A.; Hüge, J.; Purfürst, S.; Forchhammer, K.; Michel, K.-P.; Bauwe, H.; Kopka, J.; Hagemann, M. Metabolic and Transcriptomic Phenotyping of Inorganic Carbon Acclimation in the Cyanobacterium *Synechococcus elongatus* PCC 7942. *Plant Physiol.* **2011**, *155* (4), 1640−1655.

(56) Zhang, H.; Du, W.; Peralta-Videa, J. R.; Gardea-Torresdey, J. L.; White, J. C.; Keller, A.; Guo, H.; Ji, R.; Zhao, L. Metabolomics Reveals How Cucumber (*Cucumis sativus*) Reprograms Metabolites To Cope with Silver Ions and Silver Nanoparticle-Induced Oxidative Stress. *Environ. Sci. Technol.* **2018**, *52* (14), 8016−8026.

(57) Xia, J.; Sinelnikov, I. V.; Han, B.; Wishart, D. S. MetaboAnalyst 3.0—Making Metabolomics More Meaningful. *Nucleic Acids Res.* **2015**, *43* (W1), W251−W257.

(58) Jung, Y.; Ahn, Y. G.; Kim, H. K.; Moon, B. C.; Lee, A Y.; Ryu, D. H.; Hwang, G.-S. Characterization of *Dandelion* Species Using ^1H NMR- and GC-MS-Based Metabolite Profiling. *Analyst* **2011**, *136* (20), 4222−4231.

(59) Xia, J.; Wishart, D. S. MSEA: A Web-Based Tool to Identify Biologically Meaningful Patterns in Quantitative Metabolomic Data. *Nucleic Acids Res.* **2010**, *38* (Suppl_2), W71−W77.

(60) Jarvie, H. P.; Al-Obaidi, H.; King, S. M.; Bowes, M. J.; Lawrence, M. J.; Drake, A. F.; Green, M. A.; Dobson, P. J. Fate of Silica Nanoparticles in Simulated Primary Wastewater Treatment. *Environ. Sci. Technol.* **2009**, *43*, 8622.

(61) Raveh, A.; Avnimelech, Y. Total Nitrogen Analysis in Water, Soil and Plant Material with Persulphate Oxidation. *Water Res.* **1979**, *13* (9), 911−912.

(62) Liu, T.; Xiao, B.; Xiang, F.; Tan, J.; Chen, Z.; Zhang, X.; Wu, C.; Mao, Z.; Luo, G.; Chen, X.; Deng, J. Ultrasmall Copper-Based Nanoparticles for Reactive Oxygen Species Scavenging and Alleviation of Inflammation Related Diseases. *Nat. Commun.* **2020**, *11* (1), 2788.

(63) Jiang, B.; Duan, D.; Gao, L.; Zhou, M.; Fan, K.; Tang, Y.; Xi, J.; Bi, Y.; Tong, Z.; Gao, G. F.; Xie, N.; Tang, A.; Nie, G.; Liang, M.; Yan, X. Standardized Assays for Determining the Catalytic Activity and Kinetics of Peroxidase-like Nanozymes. *Nat. Protoc.* **2018**, *13* (7), 1506−1520.

(64) Zhang, M.; Wang, H.; Liu, P.; Song, Y.; Huang, H.; Shao, M.; Liu, Y.; Li, H.; Kang, Z. Biotoxicity of Degradable Carbon Dots towards Microalgae *Chlorella vulgaris*. *Environ. Sci.: Nano* **2019**, *6* (11), 3316−3323.

(65) Samari, F.; Salehipoor, H.; Eftekhar, E.; Yousefinejad, S. Low-Temperature Biosynthesis of Silver Nanoparticles Using Mango Leaf Extract: Catalytic Effect, Antioxidant Properties, Anticancer Activity and Application for Colorimetric Sensing. *New J. Chem.* **2018**, *42* (19), 15905−15916.